Journal of the Indian Chemical Society 98 (2021) 100051

Contents lists available at ScienceDirect

Journal of the Indian Chemical Society

journal homepage: www.editorialmanager.com/JINCS/default.aspx

Synthesis, antibacterial and computational studies of Halo Chalcone hybrids from 1-(2,3-Dihydrobenzo[*b*][1,4]dioxin-6-yl)ethan-1-one

Rahul A. Shinde *, Vishnu A. Adole, Bapu S. Jagdale, Bhatu S. Desale

PG Department of Chemistry, Mahatma Gandhi Vidyamandir's Arts, Science and Commerce College (Affiliated to Savitribai Phule Pune University, Pune) Manmad, Maharashtra, India

ARTICLE INFO

Keywords:
Chalcone
Antibacterial activity
1-(2,3-Dihydrobenzo[*b*][1,4]dioxin-6-yl)ethan-1-one
DFT

ABSTRACT

In an endeavor to develop antibacterial agents, a series of six 1,4-benzodioxan-6-yl substituted chalcone derivatives were synthesized by the base-catalyzed Claisen-Schmidt reaction of the 1-(2,3-dihydrobenzo[*b*][1,4]dioxin-6-yl)ethan-1-one with fluoro and chloro substituted aromatic aldehydes. The synthesized products were characterized by FT-IR, ^{1}H NMR, and ^{13}C NMR spectroscopic techniques. The density functional theory (DFT) calculations were performed using the B3LYP functional with the 6-31G(d,p) basis set for the optimization of molecular geometries and frequency calculations. The CAM-B3LYP functional with a 6-31G(d,p) basis set was used in time-dependent density functional theory (TD-DFT) calculations for the electronic absorption studies. Optimized geometries, frontier molecular orbitals, and global reactivity descriptors' specifications were computed and addressed. The simulated electronic absorption spectra were recorded in the gas phase and dichloromethane (DCM) solvent. The electronic configurations, oscillator strengths, and excited state energies were also discussed. The theoretical UV–Vis and IR vibrational analyses were equated with the experimental findings for the assignment of absorption bands. The synthesized chalcones were evaluated for *in vitro* antibacterial activities against two Gram positive bacteria (*Bacillus subtilis* and *Staphylococcus aureus*) and two Gram negative bacteria (*Escherichia coli* and *Proteus vulgaris*). The DFT simulations were correlated with the antibacterial findings and it was discovered that they were highly helpful in the designing antibacterial agents and to establish the structure–activity relationship. Theoretical calculations are in good correlation with the *in vitro* antibacterial results.

1. Introduction

Due to the excellent pharmacological exercises, the chalcones of both natural and synthetic origin have received ample attention. Continuing through the worldwide reports in every database of various recorded and awarded patents of medicinal interest, an exceedingly strong understanding is that the researchers have deeply tried to transform the concealed natural and traditional pharmacological information into advanced medications. The rapid increase in antibiotic resistance has become a notorious global epidemic, and chalcone derivatives have been seen as one of the sets of compounds that fascinate this serious public health issue for the advancement of pharmaceuticals [1–3]. Chalcones belong to a class of flavonoids and are widely distributed in plants such as fruits, vegetables, tea, and spices [4–6]. Natural and synthetic forms of chalcones are found to show various important bioactivities including anticancer [7], antimicrobial [8], antioxidant [9], anti-inflammatory [10], antitubercular [11], anti-angiogenic [12], anti-breast cancer [13]. In view of its appreciative antimicrobial activity, the chalcone framework has been utilized for chemical alteration to discover novel derivatives with improved pharmacological profiles. The majority of the chalcone moieties have produced profound interest owing to the fact that their biological properties and characteristic conjugated molecular framework and subsequently are in the focal point of consideration of drug designing. Chalcones are natural biocides and are notable intermediates in the synthesis of different heterocyclic scaffolds [14,15].

Chalcone compounds have a typical 1,3-diaryl-2-propen-1-one chemical skeleton, also known as chalconoid, which occurs as *trans* and *cis* isomers, with a thermodynamically more stable *trans* isomer. For clinical use, many chalcone-based compounds have been endorsed. Metochalcone, for example, was introduced as a choleretic treatment, while sofalcone was previously seen as an anti-ulcer and mucoprotective drug [16–18]. Conventionally chalcones can be synthesized by Claisen-Schmidt condensation; the condensation reaction between aromatic aldehydes and aromatic ketones to form α,β-unsaturated aromatic

* Corresponding author.
E-mail address: rahulshinde843@gmail.com (R.A. Shinde).

https://doi.org/10.1016/j.jics.2021.100051
Received 21 February 2021; Received in revised form 30 April 2021; Accepted 30 April 2021
0019-4522/© 2021 Indian Chemical Society. Published by Elsevier B.V. All rights reserved.

enone pharmacophore. The presence of α,β-unsaturated keto function in chalcones can undergo conjugate addition into an essential protein with a nucleophilic group, thereby conferring antimicrobial activity. Chalcones containing heterocyclic ring systems of nitrogen, oxygen, or sulphur have improved pharmacological activity. With the widespread benefits of halogenated organic compounds bearing heterocyclic ring system, we have directed our investigation in the synthesis of chalcone derivatives adhered to a heterocyclic ring containing an oxygen atom.

The field of DFT has captivated researchers because of its wide applications in structural chemistry. Utilizing DFT, several noteworthy structural parameters could be speculated [19–21]. The molecular properties like molecular structure, bond lengths, and bond angles and spectroscopic properties like UV–Vis, FT-IR, Raman, and NMR have been largely explored by using the DFT method with appropriate functional and basis set [22–25]. It has been reported that the DFT approach using B3LYP functional with suitable basis set predicts the UV–Vis and vibrational spectroscopic properties in right agreement with the experimental spectroscopic data [26–31]. The assignment of absorption bands and, as a result, the prediction of electronic and chemical properties of molecules are observed to be appropriate using the B3LYP functional with a 6-31G(d,p) basis set [32–36]. DFT has been used to research these obligatory facets in the computational study of synthesized molecules. Most notably, DFT simulations have previously been used to anticipate biological activities [37–39]. By considering all these important aspects of biologically active chalcones and computational chemistry we present here the combined study on synthesis, antibacterial and computational investigation of chloro and fluoro bearing chalcones derived from 1-(2,3-dihydrobenzo[*b*][1,4]dioxin-6-yl)ethan-1-one. In the context of the study, this is the first report on the combined exploration of antibacterial and DFT studies of the synthesized chalcones.

2. Results and discussion

2.1. Chemistry

All the chalcone derivatives synthesized (3a–3f) *via* the Claisen–Schmidt condensation reaction were characterized by FT-IR, ^{13}C NMR, and ^{1}H NMR spectroscopy, and the findings were correlated with literature data. The structures of the synthesized chalcones are given in Table 1 and their abbreviations are used for the discussion of data presented in the current research work. For compound DBDCPP-3 containing 2,6-dichlorobenzaldehyde moiety, the highest yield (95%) was obtained, whereas compound DBFPP-2 gave the lowest yield (82%). It was seen that there is an improvement in the yield when fluoro substituent is replaced by chloro substituent. In particular, as the electronegativity of halogens decreases, the yield increases. FT-IR spectra of synthesized chalcones showed the appearance of the broad intense peaks in the range of 3088–2843 cm^{-1} due to Ar-CH stretching vibrations, and intense peaks in the range of 1686–1651 cm^{-1} due to νCO stretching. The existence of a ketonic carbonyl group conjugated with the olefinic carbon-carbon double bond was affirmed from the infrared spectra as the carbonyl peak was observed at a lower wavenumber than a normal carbonyl peak. The ^{1}H NMR coupling constant analyses indicated that two hydrogen atoms of the olefinic carbon-carbon double bond were in a *trans* configuration (*J* approximately 15 Hz) [25]. The existence of two methylene (–CH_2–) groups attached to the oxygen atoms affirmed by the chemical shifts in the range 4.38–4.26 ppm in the ^{1}H NMR spectra. The signals for these two methylene groups were seen in the ^{13}C NMR spectrum in the range of 64.0–65.0 ppm. In addition, the signal which appeared as multiplets in the aromatic region (6.5–8.5 ppm) indicates the presence of aromatic protons present in the molecules. The ^{13}C NMR

Table 1
Structures and Abbreviations used.

Sr. No.	Structure of the chalcone	Name of the chalcone	Abbreviation used
1.	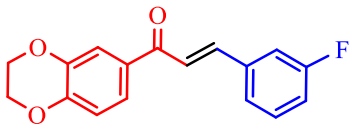	(*E*)-1-(2,3-dihydrobenzo[*b*][1,4]dioxin-6-yl)-3-(3-fluorophenyl)prop-2-en-1-one	DBFPP-1
2.	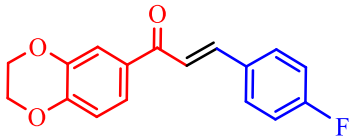	(*E*)-1-(2,3-dihydrobenzo[*b*][1,4]dioxin-6-yl)-3-(4-fluorophenyl)prop-2-en-1-one	DBFPP-2
3.	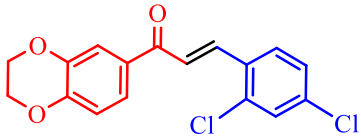	(*E*)-1-(2,3-dihydrobenzo[*b*][1,4]dioxin-6-yl)-3-(2,4-dichlorophenyl)prop-2-en-1-one	DBDCPP-1
4.	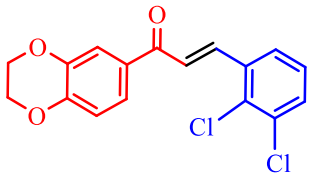	(*E*)-1-(2,3-dihydrobenzo[*b*][1,4]dioxin-6-yl)-3-(2,3-dichlorophenyl)prop-2-en-1-one	DBDCPP-2
5.	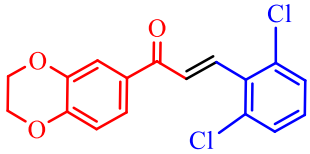	(*E*)-1-(2,3-dihydrobenzo[*b*][1,4]dioxin-6-yl)-3-(2,6-dichlorophenyl)prop-2-en-1-one	DBDCPP-3
6.	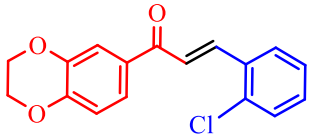	(*E*)-1-(2,3-dihydrobenzo[*b*][1,4]dioxin-6-yl)-3-(2-chlorophenyl)prop-2-en-1-one	DBCPP

signals at approximately 188.5 ppm in all synthesized chalcones were assigned carbonyl carbon. The carbonyl carbon of isolated ketone absorbs nearly at 200.0 ppm, nonetheless, the presence of α,β unsaturation, causes an upfield shift in chemical shift value, and the reasonable justification is the delocalization of charge by the benzene ring or by the double bond which increases the electron density at carbonyl carbon as compared to the isolated to the carbonyl carbon.

2.2. Computational study

The selection of a suitable basis set was an important task during the computational study. For the accurate selection of the basis set, there should be a high degree of agreement between theoretical simulations and experimental results. For the purpose of determining a suitable basis set, the experimental IR data were correlated with the theoretically computed IR data by employing the B3LYP functional with four separate basis sets: 6-31G(d,p), 6-311G(d,p), 6-311+G(d,p) and 6-311++G(d,p). During this correlation, we observed that the theoretical and experimental IR data matches appropriately with a 6-31G(d,p) basis set. Thus, optimization and frequency calculations of the studied chalcones were computed by using B3LYP functional with a 6-31G(d,p) basis set. While for TD-DFT calculations the CAM-B3LYP functional with a basis set of 6–31G(d,p) was more appropriate as there was a great agreement between the theoretical and experimental UV–Vis absorption data.

2.2.1. Molecular structure study

Six chalcone molecules synthesized from 1-(2,3-dihydrobenzo[*b*][1,4]dioxin-6-yl)ethan-1-one (Table 1) were analyzed in the current examination using the DFT method with a B3LYP functional and 6-31G(d,p) basis set to set up different structural and chemical parameters. Fig. 1 depicts the optimized molecular structures of the synthesized chalcone molecules. The highest polarity (μ = 3.42 Debye) was found in DBFPP-2 molecule and the lowest (μ = 1.61 Debye) in DBCPP molecule. The reason for the high polarity in the DBFPP-2 molecule is attributed to the presence of more electronegative fluorine atom *para* to the, α,β conjugated system. On the other hand, in the case of the DBCPP molecule, the presence of less electronegative chlorine atom at the ortho position brings about a reduction in polarity. The phenomenon of polarity is extremely crucial to foresee which compounds would enter through the lipophilic membrane of the microorganisms.

2.2.2. Frontier molecular orbitals' and global descriptors' study

The frontier molecular orbitals (FMOs) of the synthesized molecules are presented in Table 2. The highest occupied molecular orbital (HOMO) and lowest unoccupied molecular orbital (LUMO) are called as FMOs. The electron occupancy in the HOMO and LUMO are often used to predict the chemical reactivity of the molecules [40,41]. The HOMO is mainly concentrated on the 2,3-dihydrobenzo[*b*][1,4]dioxin-6-yl structure of the chalcone skeleton in all of the analyzed chalcone molecules, according to FMO pictures. This is attributed to the presence of higher electron density in the heterocyclic part of the chalcone skeleton. On the contrary, it was revealed that LUMO is primarily induced by the molecule's conjugated double bonds, and hence it is distributed through another aryl ring also. This interpretation leads to the conclusion that these chalcone molecules will facilitate aromatic electrophilic substitution reactions on the 2,3-dihydrobenzo[*b*][1,4]dioxin-6-yl structure and aromatic nucleophilic substitution reactions on another aryl ring. The electronic parameters were predicted by using HOMO and LUMO energies. The global reactivity parameters were established using Koopman's theorem to analyze the chemical behavior of the synthesized chalcone molecules [40–42]. The electronic parameters and global reactivity descriptor statistics of all six chalcone molecules are given in Table 3 and Table 4, respectively. The FMOs' calculations showed that the DBDCPP-1 and DBDCPP-2 molecules have the less HOMO-LUMO energy gap (Eg = 3.77 eV) and the DBFPP-2 molecule has the most elevated HOMO-LUMO energy gap (Eg = 3.95 eV). The rationale for this behavior is the presence of more electronegative fluorine substituent in the DBFPP-2 molecule. The lower HOMO-LUMO energy difference in the DBDCPP-1 and DBDCPP-2 molecules showed that the eventual transfer of charge occurs within the molecules. The DBCPP molecule has more reactive HOMO ($E_{HOMO} = -5.92$ eV) and DBDCPP-1 and DBDCPP-3 have less reactive HOMO ($E_{HOMO} = -6.00$ eV). This implies that DBCPP would react faster with electrophiles while DBDCPP-1 and DBDCPP-3 with a slower rate. The DBCPP molecule contains one chlorine substituent,

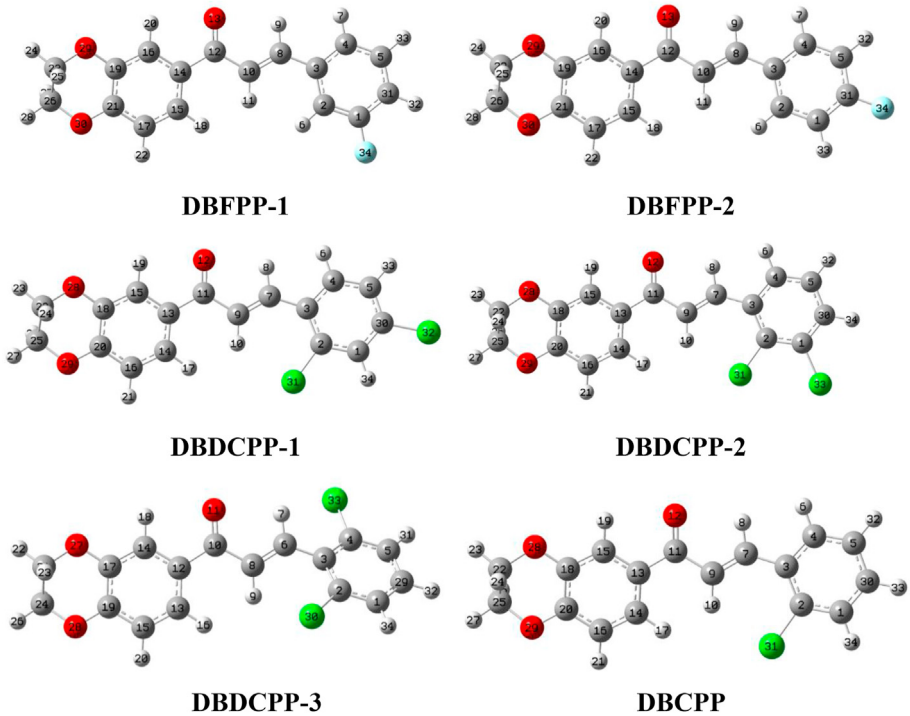

Fig. 1. Optimized molecular structures of synthesized chalcones.

Table 2
FMO of title molecules.

Entry	HOMO	LUMO
DBFPP-1	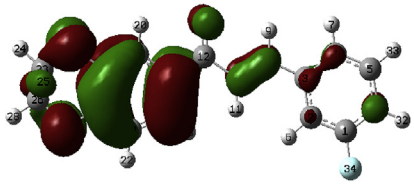	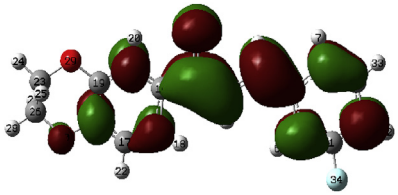
DBFPP-2	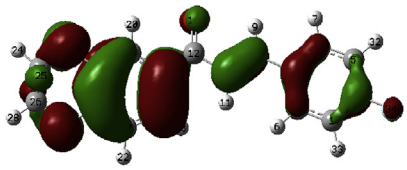	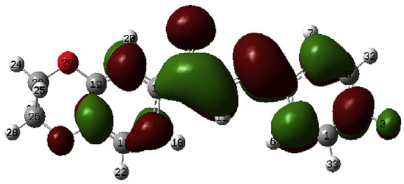
DBDCPP-1	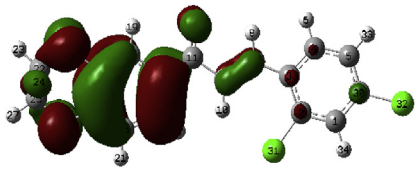	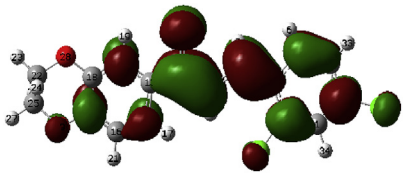
DBDCPP-2	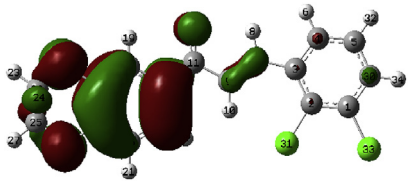	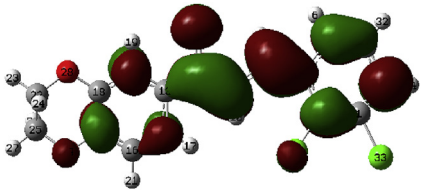
DBDCPP-3	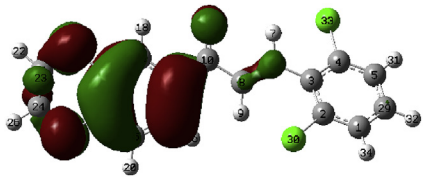	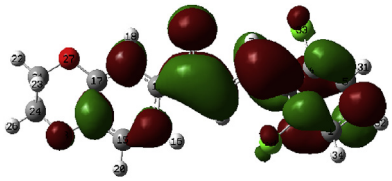
DBCPP	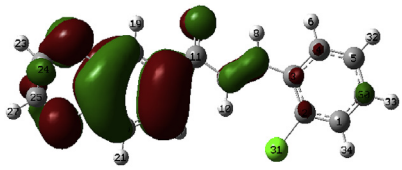	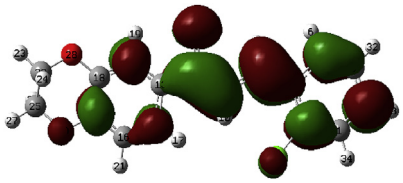

Table 3
Electronic parameters.

Entry	E_{Total} (a.u.)	E_{HOMO} (eV)	E_{LUMO} (eV)	Eg (eV)	I (eV)	A (eV)
DBFPP-1	**−981.14**	−5.98	−2.10	3.88	5.98	2.10
DBFPP-2	**−981.14**	−5.94	−1.99	3.95	5.94	1.99
DBDCPP-1	**−1801.09**	−6.00	−2.23	3.77	6.00	2.23
DBDCPP-2	**−1801.08**	−5.99	−2.22	3.77	5.99	2.22
DBDCPP-3	**−1801.08**	−6.00	−2.10	3.90	6.00	2.10
DBCPP	**−1341.49**	−5.92	−2.06	3.86	5.92	2.06

Note: $I = -E_{HOMO}$ & $A = -E_{LUMO}$.

Table 4
Global reactivity parameters.

Entry	X (eV)	η (eV)	σ (eV^{-1})	ω (eV)	Pi (eV)	ΔNmax (eV)	Dipole moment (Debye)
DBFPP-1	4.04	1.94	0.51	4.21	−4.04	2.08	2.37
DBFPP-2	3.96	1.97	0.51	3.98	−3.96	2.01	3.42
DBDCPP-1	4.11	1.88	0.53	4.49	−4.11	2.19	2.90
DBDCPP-2	4.10	1.88	0.53	4.47	−4.10	2.18	1.72
DBDCPP-3	4.05	1.95	0.51	4.20	−4.05	2.08	3.36
DBCPP	3.99	1.93	0.52	4.12	−3.99	2.07	1.61

Note: $\chi = (I + A)/2$; $\eta = (I - A)/2$; $\sigma = 1/\eta$; $\omega = Pi^2/2\eta$; $Pi = -\chi$; $\Delta Nmax = -Pi/\eta$.

while the DBDCPP-1 and DBDCPP-3 molecules have two chlorine substituents that affect the HOMO energy. The LUMO of DBDCPP-1 molecule is more reactive ($E_{LUMO} = -2.23$ eV) and that of DBFPP-2 ($E_{LUMO} = -1.99$ eV) is less reactive. In comparison to the other molecules, this demonstrated that DBDCPP-1 would react faster with nucleophiles and DBFPP-2 would react slower. The molecules with the highest ionization potential were DBDCPP-1 and DBDCPP-3 (I = 6.00 eV) and the lowest ionization potential was for the DBCPP molecule (I = 5.92 eV). The electron affinity value is higher for the DBDCPP-1 molecule (A = 2.23 eV) and lower for the DBFPP-2 molecule (A = 1.99 eV). As per the HSAB concept, the idea of the hard and soft nature of molecules is viewed as a

significant strategy for the evaluation of molecules' reactivity. Concerning to global softness, the soft molecules were DBDCPP-1 and DBDCPP-2 with a global softness value of 0.53 eV^{-1}. The absolute hardness was higher for the DBFPP-2 molecule (η = 1.97 eV). The simplicity of expulsion of an electron is constrained by its chemical potential (Pi), and it is moreover related to its electronegativity. A molecule's propensity to lose an electron increases with an increase in chemical potential value. The higher value of the global electrophilicity index defines a good electrophile, and its lower value suggests a good nucleophile. Our study on global reactivity parameters indicated that the DBDCPP-1 molecule has a higher global electrophilicity index value (ω = 4.49 eV), so the electron-accepting ability of this molecule is greater and would undergo nucleophilic attacks at a faster rate as well. The DBFPP-2 molecule, on the other hand, has a lower global electrophilicity value (ω = 3.98 eV), therefore, comparatively, it is a poor electrophile.

2.2.3. UV–visible absorption studies

The absorption wavelengths (λ in nm), oscillator strength (*f*), and configurations of DBDCPP-3 were computed using the TD-DFT method and CAM-B3LYP functional with a 6-31G(d,p) basis set for the optimized structure of DBDCPP-3. The electronic absorption data are presented in Table 5. Fig. 2 portrays the theoretical and experimental UV–Vis spectra of the DBDCPP-3. The experimental UV–Vis spectrum was taken in DCM solvent and the theoretical UV–Vis analysis was simulated in the gas phase and DCM. The theoretical and experimental UV–Vis data were compared to assign the absorption bands. The theoretical UV–Vis spectral investigation was performed up to two singlet excited states for both gas phase and DCM. We found an ideal correlation between the theoretical and experimental results. The gas phase UV–Vis simulation was observed at 360.27 and 296.00 nm for the first and second singlet excited states respectively. Then again, the computations in the DCM were found at 347.49 and 306.65 nm for the first and second singlet excited states respectively. This perception predicts that a hypsochromic shift was observed for the first excited state and a bathochromic for the second excited state. The experimental UV–Vis results in DCM were found at 334.20 and 295.77 nm for the n-π* and π-π* electronic excitations respectively. This outcome unmistakably matched with the theoretical simulations. For the n-π* electronic excitation ground state was found to be more polar than excited state and therefore in DCM solvent hypsochromic shift was observed. On the contrary, the excited state was observed to be more polar than a ground state for π-π* electronic excitation and thus showed a bathochromic shift in DCM solvent. The gas phase excitation was to be composed of four configurations in both first and second singlet excited states and three configurations are obtained for the electronic excitations in DCM.

2.2.4. Vibrational analysis

In Fig. 3, the theoretical and experimental IR spectra of the DBDCPP-3 molecule are presented. The comparison of selected experimental and scaled theoretical vibrational bands of the DBDCPP-3 molecule is presented in Table 6. Different sorts of functionality present in the DBDCPP-3 molecule were assigned to the various absorption bands. In order to assign a specific bond to a specific IR value, various vibrational bands were theoretically and experimentally correlated. The stretching vibrations of sp^3-C-H were found at approximately at 2900-3000 cm^{-1}. The

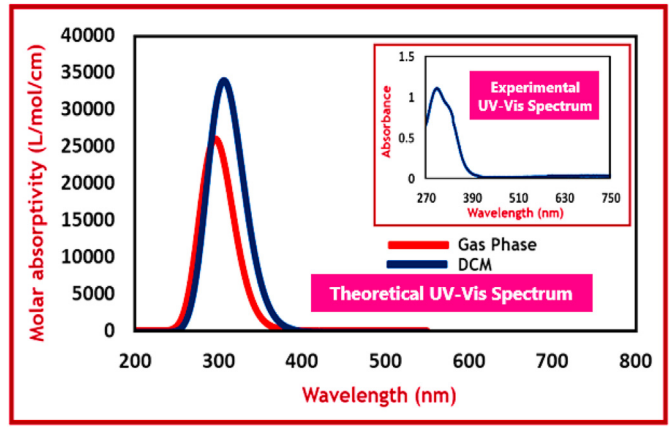

Fig. 2. UV–Vis spectra of the DBDCPP-3.

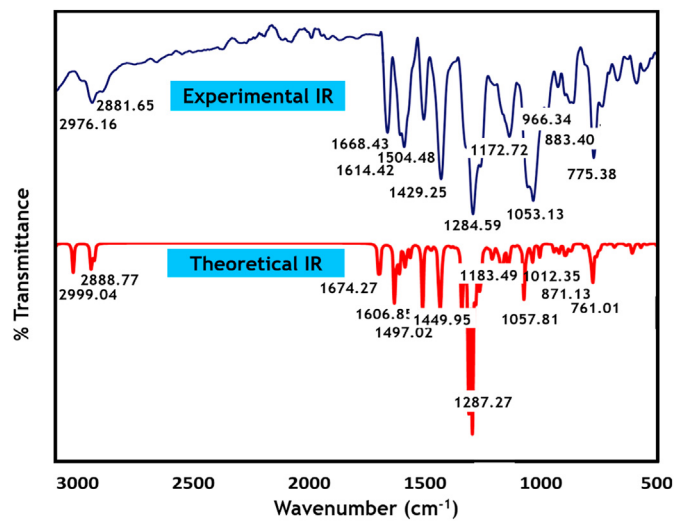

Fig. 3. Theoretical and experimental IR spectra of the DBDCPP-3 molecule.

vibrational band below 1700 cm^{-1} apparently demonstrated the presence of a carbonyl group of conjugated ketones. At 1668.43 cm^{-1}, the IR frequency of a carbonyl group was noticed. The conjugative effect on the ketone carbonyl caused a significant decrease in carbonyl frequency. With amplitude of 127.86 km mol^{-1}, the scaled carbonyl vibrational band was observed at 1674.27 cm^{-1}. This demonstrated a very strong agreement between experimental and theoretical carbonyl frequency. At almost 1620 cm^{-1}, the conjugated olefin bond showed a stretching band. At 1606.85 cm^{-1}, the scaled vibrational band was obtained. The DBDCPP-3 molecule was found to show olefinic C═C stretching frequency at 1614.42 cm^{-1} that suggested the vibrational frequencies were found in good accordance with each other. For the structural parts of the title compounds, vibrational bands such as stretching, deformation, in-plane bending, out of plane bending, scissoring were assigned. The experimental vibrational data have shown a strong correlation with the

Table 5
Absorption wavelengths (λ in nm), oscillator strength (*f*), and configurations of DBDCPP-3 computed using TD-DFT CAM-B3LYP/6-31G(d,p) level of theory.

State	Gas Phase			DCM		
	Configuration	λ, (nm)	Oscillator strength (*f*)	Configuration	λ, (nm)	Oscillator strength (*f*)
1	83 -> 87 83 -> 89 83 -> 92 85 -> 87	360.27	0.0001	82 -> 87 82 -> 89 82 -> 92	347.49 **(334.20)**	0.0004
2	83 -> 87	296.00	0.6406	85 -> 87	306.65 **(295.77)**	0.0004
	85 -> 87			86 -> 87		
	86 -> 87			86 -> 89		
	86 -> 89					

Table 6
Comparison between selected experimental and scaled theoretical vibrational assignments of DBDCPP-3 molecule calculated using DFT method with B3LYP/6-31G(d,p) level of theory.

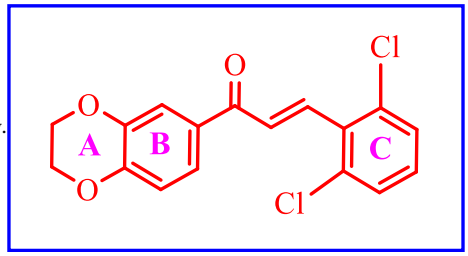

Mode	Computed frequencies (cm^{-1})	IR Intensity ($km.mol^{-1}$)	Observed frequencies (cm^{-1})	Assignments
87	2999.04	40.93	2976.16	ν C21–H
86	2888.77	50.46	2881.65	ν *sym* C24–H_2
84	1674.27	127.86	1668.43	ν C=O
83	1606.85	160.35	1614.42	ν C6=C8 (olefin)
79	1497.02	28.91	1504.48	ν C1=C29 + v C2=C3
76	1449.95	3.41	1429.25	scis C24–H_2 + scis C27–H_2
68	1287.27	350.85	1284.59	β C6–H
61	1183.49	47.29	1172.72	β Ar–H (ring B)
52	1057.81	29.78	1053.13	def ring A + def ring B
51	1012.35	53.38	996.34	β C14–H
44	871.13	0.11	883.40	γ C5–H
39	761.01	15.10	775.38	def ring A + def ring B + def ring C

Note: ν -stretching; sym-symmetric; def-deformation; β-in-plane bending; γ-out of plane bending; scis - scissoring.

simulated vibrational data, which led to the accurate assignment of the vibrational bands to different types of functionality present in the DBDCPP-3 molecule.

2.3. Antibacterial study

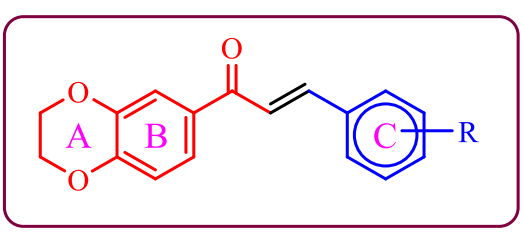

During antibacterial screening for chalcone compounds (3a–3f), Gram positive bacteria (*Bacillus subtilis* and *Staphylococcus aureus*) and Gram negative bacteria (*Escherichia coli* and *Proteus vulgaris*) were used. The well-known agar diffusion assay is used to access the antibacterial activities of the synthesized compounds. The synthesized chalcone compounds showed promising antibacterial activity against used strains; particularly the compounds DBFPP-1, DBFPP-2, DBDCPP-3 and DBCPP have shown better antimicrobial activity. For antibacterial activity screening, chloramphenicol was used as a standard drug candidate and DMSO as a control. The result of antibacterial screening is tabulated in Table 7. The aim of this antibacterial analysis was to examine how chloro and fluoro substituents in ring C influence the antibacterial activity of the synthesized chalcone compounds. It has been reported in the past that the LUMO energies can be used to predict the antibacterial activities of the molecules. Molecules with less negative LUMO energy are often resulting in higher biological activity than molecules with more negative LUMO energy, [37,39]. On the basis of DFT calculations, one can predict

Table 7
Antibacterial activity of the synthesized chalcone derivatives.

Sr. No.	Entry	*E. coli*	*P. vulgaris*	*S. aureus*	*B. subtilis*
1	DBFPP-1	+++	−	−	+++
2	DBFPP-2	−	++	−	++
3	DBDCPP-1	−	−	−	−
4	DBDCPP-2	−	−	−	−
5	DBDCPP-3	++	++	+++	++
6	DBCPP	++	+++	++	++
Control	**DMSO**	−	−	−	−
Standard	**Chloramphenicol**	++++	++++	++++	++++

Note: + = less than 5 mm; ++ = 5–10 mm; +++ = 10–15 mm; ++++ = more than 15 mm; − = No zone of inhibition.

the LUMO energies of the molecules and consequently can foresee its effect on the antibacterial activities of the molecules. The compounds DBDCPP-1 and DBDCPP-2 are having LUMO energies −2.23 eV and −2.22 eV respectively (Table 3). These two compounds, as anticipated, showed no antibacterial activity as their LUMO energies are more negative. Similarly, there is a great connection between antibacterial activity and global softness values. Molecules with high global softness values were unable to penetrate the bacterial cell wall, making them biologically ineffective. Both DBDCPP-1 and DBDCPP-2 have a higher global softness value (ω = 0.53 eV). The other four molecules have lower global softness values than these two, suggesting that they are more powerful antibacterial agents. The presence of the fluoro substituent in ring C has a moderate effect on the stimulation of antibacterial action, according to the antibacterial evaluation of the synthesized compounds. The compounds DBFPP-1 and DBFPP-2 are found to exhibit a moderate antibacterial effect. The compound DBFPP-1 has shown antibacterial action against Gram negative bacteria *Escherichia coli* and Gram positive bacteria *Bacillus subtilis*. The compound DBFPP-2, on the other hand, was shown to have antibacterial activity against both Gram negative and Gram positive bacteria, namely *Proteus vulgaris* and *Staphylococcus aureus*. Nonetheless, it is worth noting, that both of these chalcone compounds have antibacterial functions against Gram positive as well as Gram negative bacteria. The structure-activity relationship revealed here that the presence of a chloro substituent at the ortho position of the aryl ring (ring C) was designed to boost antibacterial activity against all tested bacterial strains. On the contrary, the C-4 and C-3 positions of chloro substituent attributed to diminishing antibacterial activity against the tested Gram positive and Gram negative bacterial strains. The combination of C-2 position with C-3 and C-4 positions for chloro substituent was found to show negative antibacterial potential. In this research, it was established that when the chloro substituent is present at both ortho positions (C-2 and C-6), the antibacterial propensity increases significantly. The compounds DBDCPP-1 and DBDCPP-2 were found to have no biological impact on microbial strains that were tested. The compounds DBDCPP-3 and DBDCPP have bactericidal activity across a wide range of bacteria. The compounds DBDCPP-3 and DBDCPP have shown bactericidal effects against both Gram positive and Gram negative bacterial strains. The compound DBDCPP-3 was found to exhibit strong bacterial action against Gram positive bacteria *Staphylococcus aureus* and on the other hand compound DBDCPP was found to show strong bacterial action against Gram negative bacteria *Proteus vulgaris*.

3. Conclusions

In conclusion, this work reports the synthesis, computational and antibacterial studies of six chalcone derivatives derived from 1-(2,3-dihydrobenzo[*b*][1,4]dioxin-6-yl)ethan-1-one. The synthesized compounds were obtained in good to excellent yields. The structures were affirmed using FT-IR and NMR spectral analysis. The ^{1}HNMR study revealed a *trans* configuration for the olefinic double bond. The B3LYP functional with 6–31G(d,p) basis set was used to perform DFT calculations for the optimization of molecular geometries and frequency

calculations. For the electronic absorption studies, TD-DFT calculations were performed using the CAM-B3LYP functional with the 6-31G(d,p) basis set. The optimized structures uncovered DBFPP-2 molecule as more polar molecule. The FMO analysis indicated the lower HOMO-LUMO energy gap in DBDCPP-1 and the DBDCPP-2 molecules suggesting inevitable electron transfer with maximum electronic charge. The correlation between theoretical and experimental UV–Vis results was found to be ideal and correct assignments of UV–Vis bands were obtained. The UV–Vis spectral investigation of DBDCPP-3 revealed that the first singlet excited state corresponds to the n-π* electronic transition and the second to π-π* electronic transition. Additionally, a good correlation between theoretical and experimental IR data was found. The scrutiny of the antibacterial results uncovered that in fluorinated chalcones, the compound bearing a 3-fluoro substituent was more active against chosen bacterial strains than chalcone bearing 4-fluoro substituent. Likewise in chlorinated chalcones chorine at the C-2 position showed strong activity against both Gram positive and Gram negative bacteria and the antibacterial potential was enhanced by the addition of another chlorine atom at the C-6 position. We conclude that the present research on computational and antibacterial examination of studied chalcone derivatives would be extremely useful in the development of antibacterial agents with fluoro and chloro substituents in the aryl portion of the chalcone structure.

4. Materials and methods

4.1. General remarks

The chemicals (Make-SD fine chemicals and Avra synthesis) with high purity were purchased from the Sigma laboratory, Nashik, and were utilized accordingly. On the Shimadzu spectrometer, the FT-IR spectra of the synthesized compounds were recorded using a KBr disc technique. The NMR analysis was performed on advanced multinuclear FT-NMR Spectrometer model. In chloroform-d, the compounds were dissolved. Chemical shifts were recorded in ppm using tetramethylsilane (TMS) as an internal standard. The reactions were analyzed using thin-layer chromatography on a silica gel coated with fluorescent indicator F254 on the Merck Aluminium TLC plate. All the glass components were cleaned and dried in the oven prior to use.

4.2. Experimental procedure

Equimolar combination of 1-(2,3-dihydrobenzo[*b*][1,4]dioxin-6-yl) ethan-1-one (1) and aromatic aldehydes (2) were added to an appropriate amount of ethanol taken in a 50 mL conical flask. To this, NaOH (30%) was added and the resulting mixture was stirred for 2–3 h to get the desired chalcones. Thin layer chromatography (n-hexane/EtOAc [8:2]) was used continuously to monitor the completion of the reaction. The alkaline reaction mass was neutralized by adding appropriate amount of dilute HCl. The crude products were obtained after filtration were dried and recrystallized using ethanol solvent. Using FT-IR, ^{1}HNMR and ^{13}C NMR spectral techniques, the synthesized products (3a-3f) were characterized. The reaction is presented in Scheme 1.

4.3. Spectral analysis

4.3.1. (E)-1-(2,3-dihydrobenzo[b][1,4]dioxin-6-yl)-3-(3-fluorophenyl) prop-2-en-1-one (DBFPP-1 or 3a)

Yield- 86%; white solid, M.P.: 95 °C; FT-IR (KBr, cm^{-1}): 3064.89, 2995.45, 2887.44, 1651.07, 1583.56, 1502.55, 1427.32, 1255.66, 1209.37, 1149.57, 1053.13, 979.84, 900.76, 879.54, 810.10, 734.88, 661.58, 582.50, 528.50, 464.84; ^{1}H NMR (500 MHz, $CDCl_3$, δ): 7.76 (d, J = 15.6 Hz, 1H), 7.70–7.63 (m, 2H), 7.59 (d, J = m, 2H), 7.47 (d, J = 15.6 Hz, 1H), 7.29–7.25 (m, 2H), 7.00–6.94 (m, 1H), 4.38–4.33 (m, 2H), 4.33–4.28 (m, 2H); ^{13}C NMR (126 MHz, $CDCl_3$, δ): 188.21, 150.44, 148.14, 143.51, 142.27, 133.67, 131.71, 129.79,122.73, 122.52, 121.41, 121.21, 119.36, 118.09, 117.40, 77.29, 77.04, 76.78, 64.75, 64.17.

4.3.2. (E)-1-(2,3-dihydrobenzo[b][1,4]dioxin-6-yl)-3-(4-fluorophenyl) prop-2-en-1-one (DBFPP-2 or 3b)

Yield- 82%; white solid, M.P.: 101 °C; FT-IR (KBr, cm^{-1}): 3088.03, 2922.16, 2843.07, 1685.79, 1579.70, 1419.61, 1253.73, 1149.57, 1055.06, 1012.63, 883.40, 808.17, 723.31, 671.23, 528.50, 457.13; ^{1}H NMR (500 MHz, $CDCl_3$, δ): 7.74 (d, J = 15.7 Hz, 1H), 7.62–7.57 (m, 2H), 7.49 (d, J = 15.6 Hz, 1H), 7.43–7.36 (m, 2H), 7.36–7.30 (m, 1H), 7.15–7.05 (m, 1H), 6.97 (m, 1H), 4.37–4.33 (m, 2H), 4.33–4.29 (m, 2H); ^{13}C NMR (126 MHz, $CDCl_3$, δ): 188.23, 164.04, 162.08, 148.15, 143.52, 142.62, 137.35, 131.69, 130.52, 130.46, 124.51, 122.91, 122.75, 118.10, 117.40, 117.12, 114.52, 64.75, 64.16.

4.3.3. (E)-3-(2,4-dichlorophenyl)-1-(2,3-dihydrobenzo[b][1,4]dioxin-6-yl) prop-2-en-1-one (DBDCPP-1 or 3c)

Yield- 94%; faint yellow white solid, M.P.: 154 °C; FT-IR (KBr, cm^{-1}): 2977.07, 1670.35, 1545.51, 1423.12, 1314.07, 1118.71, 1056.99, 893.04, 815.89, 667.31, 590.22, 466.52; ^{1}H NMR (500 MHz, $CDCl_3$, δ): 8.08 (d, J = 15.7 Hz, 1H), 7.67 (m, 1H), 7.61–7.54 (m, 2H), 7.47 (m, 1H), 7.43 (s, 1H), 7.30 (m, 1H), 6.96 (d, J = 15.7 Hz, 1H), 4.38–4.32 (m, 2H), 4.31 (m, 2H); ^{13}C NMR (126 MHz, $CDCl_3$, δ): 188.10, 148.22, 143.54, 138.64, 136.28, 136.02, 132.04, 131.54, 130.13, 128.49, 127.53, 124.75, 122.84, 118.16, 117.40, 64.75, 64.16.

4.3.4. (E)-3-(2,3-dichlorophenyl)-1-(2,3-dihydrobenzo[b][1,4]dioxin-6-yl) prop-2-en-1-one (DBDCPP-2 or 3d)

Yield- 93%; faint yellow white solid, M.P.: 140 °C; FT-IR (KBr, cm^{-1}): 2978.09, 2879.72, 1670.35, 1506.41, 1413.82, 1354.03, 1284.59, 1172.72, 1055.06, 960.55, 889.18, 783.10, 725.23, 626.87, 462.92, 422.41, 401.19; ^{1}H NMR (500 MHz, $CDCl_3$, δ): 8.14 (d, J = 15.6 Hz, 1H), 7.63 (m, 1H), 7.60 (m, 1H), 7.58 (m, 1H), 7.50 (m, 1H), 7.43 (d, J = 15.6 Hz, 1H), 7.26 (m, 1H), 7.00–6.93 (m, 1H), 4.38–4.32 (m, 2H), 4.32–4.28 (m, 2H); ^{13}C NMR (126 MHz, $CDCl_3$, δ): 188.14, 148.25, 143.55, 139.81, 135.86, 134.07, 133.44, 131.48, 127.37, 125.89, 125.64, 122.88, 118.20, 117.41, 64.75, 64.16.

4.3.5. (E)-3-(2,6-dichlorophenyl)-1-(2,3-dihydrobenzo[b][1,4]dioxin-6-yl) prop-2-en-1-one (DBDCPP-3 or 3e)

Yield- 95%; white solid, M.P.: 129 °C; FT-IR (KBr, cm^{-1}): 2976.16, 2881.65, 1668.43, 1614.42, 1504.48, 1429.25, 1284.59, 1172.72, 1053.13, 966.34, 883.40, 775.38, 729.09, 468.70; ^{1}H NMR (500 MHz, $CDCl_3$, δ): 7.83 (d, J = 16.1 Hz, 1H), 7.65 (s, 1H), 7.62–7.56 (m, 2H), 7.38 (d, J = 8.1 Hz, 2H), 7.20 (t, J = 8.1 Hz, 1H), 6.96 (d, J = 8.1 Hz, 1H), 4.36–4.32 (m, 2H), 4.32–4.28 (m, 2H); ^{13}C NMR (126 MHz, $CDCl_3$, δ): 188.29, 148.25, 143.51, 137.16, 135.19, 132.81, 131.48, 130.27, 129.73, 128.85, 123.00, 118.28, 117.42, 64.75, 64.14.

4.3.6. (E)-3-(2-chlorophenyl)-1-(2,3-dihydrobenzo[b][1,4]dioxin-6-yl) prop-2-en-1-one (DBCPP or 3f)

Yield- 92%; pale yellow solid, M.P.: 160 °C; FT-IR (KBr, cm^{-1}): 2975.66, 1671.85, 1605.49, 1429.25, 1371.39, 1278.81, 1201.65, 1118.71, 962.34, 831.32, 781.17, 725.23, 665.44, 526.47, 470.63; ^{1}H NMR (500 MHz, $CDCl_3$, δ): 8.16 (d, J = 15.7 Hz, 1H), 7.77–7.71 (m, 1H), 7.63–7.56 (m, 2H), 7.49–7.42 (m, 2H), 7.35–7.29 (m, 2H), 6.96 (d, J = 8.2 Hz, 1H), 4.37–4.28 (m, 4H); ^{13}C NMR (126 MHz, $CDCl_3$, δ): 188.42, 148.09, 143.49, 139.91, 135.43, 133.42, 131.67, 131.00, 130.28, 127.76, 127.04, 124.50, 122.82, 118.16, 117.34, 64.72, 64.14.

4.4. Computational methods

The geometry optimization of the studied chalcones were done using DFT method with B3LYP (Becke three parameter Lee–Yang–Parr) exchange-correlation functional with a 6-31G(d,p) basis set. The frequency calculation was done using optimized structures with B3LYP

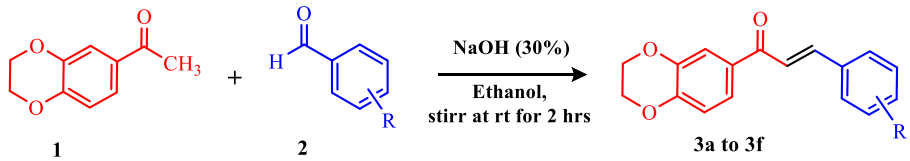

Scheme 1. Synthesis of the chalcones.

functional and 6-31G(d,p) basis set. The vibrational wavenumbers were scaled by using a scaling factor of 0.96 [27]. The simulated electronic absorption spectra were computed both in gas phase and DCM. The electronic configurations, oscillator strengths, coefficients and excited state energies were also explored using TD-DFT method and CAM-B3LYP/6-31G(d,p) computations. The energy values, ionization potential, electron affinity, electronegativity, chemical hardness and softness, global electrophilicity, and chemical potential were calculated by using highest occupied molecular orbital and lowest unoccupied molecular orbital. All calculations were performed using the Gaussian 03 package [43].

4.5. Antimicrobial evaluation

The Agar diffusion assay (Disc diffusion method, Disc size 6 mm) was used access the antimicrobial activities [44,45]. Concentration of compounds stock solution [1000 μg per mL] of each compound was prepared in distilled water. Assay carried out by taking concentration 100 microrgram per disk. Microbiological media used for bacteria is Nutrient agar (Hi-media); composition (gL^{-1}): sodium chloride, 5.0; beef extract 10.0; peptone 10.0 (pH 7.2). Microbiological media for fungi is potato dextrose agar (all ingredients of Hi media); composition (gL-1): potatoes infusion, 200; dextrose, 20; Agar, 15; final pH (at 25 °C) 5.6 ± 0.2. Chloramphenicol was used as a standard for antibacterial evaluation and Amphotericin-B for antifungal screening. Antibacterial screening was performed against *Escherichia coli* (NCIM 2109), *Proteus vulgaris* (NCIM 2172), *Staphylococcus aureus* (NCIM 2079), and *Bacillus subtilis* (NCIM 2063) [where NCIM: National Collection of Industrial Microorganisms, National Chemical Laboratory (NCL), Pune, India].

Compliance with ethical standards

On behalf of all authors, the corresponding author states that there is no conflict of interest.

Declaration of competing interest

The authors declare that they have no known competing financial interests or personal relationships that could have appeared to influence the work reported in this paper.

Acknowledgements

Authors acknowledge central instrumentation facility, Savitribai Phule Pune University, Pune for NMR and CIC, KTHM College, Nashik for FT-IR spectral analysis. Authors would also like to thank Arts, Science and Commerce College, Manmad for permission and providing necessary research facilities. Authors would like to express their sincere and humble appreciation to Prof. (Dr.) Arun B. Sawant for Gaussian study. Prof. Mahesh Patil is gratefully acknowledged for the antibacterial studies. Dr. Aapoorva Hiray, Coordinator, MG Vidyamandir institute, is gratefully acknowledged for Gaussian package.

Appendix A. Supplementary data

Supplementary data to this article can be found online at https://doi.org/10.1016/j.jics.2021.100051.

References

[1] Yin H, Dong J, Cai Y, Shi X, Wang H, Liu G, Tang Y, Liu J, Ma L. Design, synthesis and biological evaluation of chalcones as reversers of P-glycoprotein-mediated multidrug resistance. Eur. J. Med. Chem. 2019;180:350–66.
[2] da Cunha Xavier J, de Queiroz Almeida-Neto FW, da Silva PT, de Sousa AP, Marinho ES, Marinho MM, Rocha JE, Freitas PR, de Araújo ACJ, Freitas TS, Nogueira CES. Structural characterization, DFT calculations, ADMET studies, antibiotic potentiating activity, evaluation of efflux pump inhibition and molecular docking of chalcone (E)-1-(2-hydroxy-3,4,6-trimethoxyphenyl)-3-(4-methoxyphenyl) prop-2-en-1-one. J. Mol. Struct. 2021;1227:129692.
[3] Božić DD, Milenković M, Ivković B, Cirković I. Antibacterial activity of three newly-synthesized chalcones & synergism with antibiotics against clinical isolates of methicillin-resistant Staphylococcus aureus. Indian J. Med. Res. 2014;140:130.
[4] Rammohan A, Reddy JS, Sravya G, Rao CN, Zyryanov GV. Chalcone synthesis, properties and medicinal applications: a review. Environ. Chem. Lett. 2020;18:433–58.
[5] Gaonkar SL, Vignesh UN. Synthesis and pharmacological properties of chalcones: a review. Res. Chem. Intermed. 2017;43:6043–77.
[6] K Sahu N, S Balbhadra S, Choudhary J, V Kohli D. Exploring pharmacological significance of chalcone scaffold: a review. Curr. Med. Chem. 2012;19:209–25.
[7] Riaz S, Iqbal M, Ullah R, Zahra R, Chotana GA, Faisal A, Saleem RSZ. Synthesis and evaluation of novel α-substituted chalcones with potent anti-cancer activities and ability to overcome multidrug resistance. Bioorg. Chem. 2019;87:123–35.
[8] Burmaoglu S, Algul O, Gobek A, Aktas Anil D, Ulger M, Erturk BG, Kaplan E, Dogen A, Aslan G. Design of potent fluoro-substituted chalcones as antimicrobial agents. J. Enzym. Inhib. Med. Chem. 2017;32:490–5.
[9] Mathew B, Adeniyi AA, Joy M, Mathew GE, Singh-Pillay A, Sudarsanakumar C, Soliman ME, Suresh J. Anti-oxidant behavior of functionalized chalcone-a combined quantum chemical and crystallographic structural investigation. J. Mol. Struct. 2017;1146:301–8.
[10] Bhale PS, Chavan HV, Dongare SB, Shringare SN, Mule YB, Nagane SS, Bandgar BP. Synthesis of extended conjugated indolyl chalcones as potent anti-breast cancer, anti-inflammatory and antioxidant agents. Bioorg. Med. Chem. Lett 2017;27:1502–7.
[11] Anandam R, Jadav SS, Ala VB, Ahsan MJ, Bollikolla HB. Synthesis of new C-dimethylated chalcones as potent antitubercular agents. Med. Chem. Res. 2018;27:1690–704.
[12] Mirossay L, Varinská L, Mojžiš J. Antiangiogenic effect of flavonoids and chalcones: an update. Int. J. Mol. Sci. 2018;19:27.
[13] Lee KP, Beak S, Park JS, Kim YJ, Kim KN, Kim SR, Yoon MS. Antibreast cancer activity of aspirin-conjugated chalcone polymeric micelles. Macromol. Res. 2021;29:105–10.
[14] Mt Albuquerque H, Mm Santos C, As Cavaleiro J, Ms Silva A. Chalcones as versatile synthons for the synthesis of 5-and 6-membered nitrogen heterocycles. Curr. Org. Chem. 2014;18:2750–75.
[15] Nair D, Pavashe P, Katiyar S, Namboothiri IN. Regioselective synthesis of pyrazole and pyridazine esters from chalcones and α-diazo-β-ketoesters. Tetrahedron Lett. 2016;57:3146–9.
[16] Wang C, Wu P, Shen XL, Wei XY, Jiang ZH. Synthesis, cytotoxic activity and drug combination study of tertiary amine derivatives of 2′,4′-dihydroxyl-6′-methoxyl-3′,5′-dimethylchalcone. RSC Adv. 2017;7:48031–8.
[17] Goyal K, Kaur R, Goyal A, Awasthi R. Chalcones: a review on synthesis and pharmacological activities. J. Appl. Pharmaceut. Sci. 2021;11:1–14.
[18] Gomes MN, Muratov EN, Pereira M, Peixoto JC, Rosseto LP, Cravo PV, Andrade CH, Neves BJ. Chalcone derivatives: promising starting points for drug design. Molecules 2017;22:1210.
[19] Asadi Z, Esrafili MD, Vessally E, Asnaashariisfahani M, Yahyaei S, Khani A. A structural study of fentanyl by DFT calculations, NMR and IR spectroscopy. J. Mol. Struct. 2017;1128:552–62.
[20] Humphries TD, Sirsch P, Decken A, McGrady GS. A structural study of bis-(trimethylamine)alane, $AlH_3{\cdot}2NMe_3$, by variable temperature X-ray crystallography and DFT calculations. J. Mol. Struct. 2009;923:13–8.
[21] Raja M, Muhamed RR, Muthu S, Suresh M. Synthesis, spectroscopic (FT-IR, FT-Raman, NMR, UV–Visible), NLO, NBO, HOMO-LUMO, Fukui function and molecular docking study of (E)-1-(5-bromo-2-hydroxybenzylidene) semicarbazide. J. Mol. Struct. 2017;1141:284–98.
[22] Karthikeyan N, Prince JJ, Ramalingam S, Periandy S. Spectroscopic [FT-IR and FT-Raman] and theoretical [UV–Visible and NMR] analysis on α-Methylstyrene by DFT calculations. Spectrochim. Acta Mol. Biomol. Spectrosc. 2015;143:107–19.

[23] Dhonnar SL, Adole VA, Sadgir NV, Jagdale BS. Structural, spectroscopic (UV-vis and IR), electronic and chemical reactivity studies of (3,5-diphenyl-4,5-dihydro-1H-pyrazol-1-yl)(phenyl)methanone. Phys. Chem. Res. 2021;9:193–209.
[24] Adole VA, Waghchaure RH, Pathade SS, Patil MR, Pawar TB, Jagdale BS. Solvent-free grindstone synthesis of four new (*E*)-7-(arylidene)-indanones and their structural, spectroscopic and quantum chemical study: a comprehensive theoretical and experimental exploration. Mol. Simulat. 2020;46:1045–54.
[25] Adole VA, Jagdale BS, Pawar TB, Sagane AA. Ultrasound promoted stereoselective synthesis of 2,3-dihydrobenzofuran appended chalcones at ambient temperature. S. Afr. J. Chem. 2020;73:35–43.
[26] Khadri A, Bouchene R, Bouacida S, Sid A, Alswaidan IA, Ramasami P. Synthesis, structural, thermal, Hirshfeld surface and DFT studies on a new hybrid compound: bis[4-(dimethylamino)pyridinium]tetrachloridomanganate(II). J. Coord. Chem. 2020;73:609–21.
[27] Adole VA, Pawar TB, Jagdale BS. DFT computational insights into structural, electronic and spectroscopic parameters of 2-(2-Hydrazineyl)thiazole derivatives: a concise theoretical and experimental approach. J. Sulphur Chem. 2021;42:131–48.
[28] Pathade SS, Jagdale BS. Experimental and computational investigations on the molecular structure, vibrational spectra, electronic properties, FMO and mep analyses of 4,6-Bis(4-Fluorophenyl)-5,6-dihydropyrimidin-2(1H)-one: a DFT insight. Phys. Chem. Res. 2020;8:671–87.
[29] Sadgir NV, Dhonnar SL, Jagdale BS, Sawant AB. Synthesis, spectroscopic characterization, XRD crystal structure, DFT and antimicrobial study of (2E)-3-(2,6-dichlorophenyl)-1-(4-methoxyphenyl)-prop-2-en-1-one. SN Appl. Sci. 2020;2:1–12.
[30] Devi KS, Subramani P, Parthiban S, Sundaraganesan N. One-pot synthesis, spectroscopic characterizations, quantum chemical calculations, docking and cytotoxicity of 1-((dibenzylamino)methyl)pyrrolidine-2,5-dione. J. Mol. Struct. 2020;1203:127403.
[31] Adole VA, Jagdale BS, Pawar TB, Sawant AB. Experimental and theoretical exploration on single crystal, structural, and quantum chemical parameters of (*E*)-7-(arylidene)-1,2,6,7-tetrahydro-8H-indeno[5,4-b]furan-8-one derivatives: a comparative study. J. Chin. Chem. Soc. 2020;67:1763–77.
[32] Rajamani P, Vijayakumar V, Nagaraaj P, Sundaraganesan N. Synthesis, characterization, spectroscopic, DFT and molecular docking studies of 3-(3,4-dihydroxyphenyl)-1-phenyl-3-(Phenylamino)Propan-1-one. Polycycl. Aromat. Comp. 2020:1–21.
[33] Mariappan G, Sundaraganesan N. FT-IR, FT-Raman spectra, density functional computations of the vibrational spectra, molecular geometry, conformational stability and some molecular properties of 1-Bromo-2,3-dimethoxynaphthalene. J. Mol. Struct. 2014;1074:51–61.
[34] Pradeepa SJ, Sundaraganesan N. Spectroscopic and molecular structure investigations of 9-vinylcarbazole by DFT and ab initio method. Spectrochim. Acta A Mol. Biomol. Spectrosc. 2015;136:690–9.
[35] Mariappan G, Sundaraganesan N. Structural, vibrational, electronic and NMR spectral analysis of benzyl phenyl carbonate. Spectrochim. Acta A Mol. Biomol. Spectrosc. 2013;110:169–78.
[36] Govindarasu K, Kavitha E, Sundaraganesan N, Suresh M, Padusha MSA. Synthesis, structural and spectral analysis of (E)-N′-(4-Methoxybenzylidene) pyridine-3-carbohydrazide dihydrate by density functional theory. Spectrochim. Acta A Mol. Biomol. Spectrosc. 2015;135:1123–36.
[37] Khan SA, Asiri AM, Zayed ME, Parveen H, Aqlan FM, Sharma K. Microwave-assisted synthesis, characterization, and density functional theory study of biologically active ferrocenyl bis-pyrazoline and bis-pyrimidine as organometallic macromolecules. J. Heterocycl. Chem. 2019;56:312–8.
[38] Pitchumani Violet Mary C, Shankar R, Vijayakumar S. Theoretical insights into the metal chelating and antimicrobial properties of the chalcone based Schiff bases. Mol. Simulat. 2019;45:636–45.
[39] Khan SA, Asiri AM, Al-Ghamdi NSM, Asad M, Zayed ME, Elroby SA, Aqlan FM, Wani MY, Sharma K. Microwave assisted synthesis of chalcone and its polycyclic heterocyclic analogues as promising antibacterial agents: in vitro, in silico and DFT studies. J. Mol. Struct. 2019;1190:77–85.
[40] Rathi P, Khanna R, Jaswal VS. Quantum parameters based study of some heterocycles using density functional theory method: a comparative theoretical study. J. Chin. Chem. Soc. 2020;67:213–7.
[41] Shinde RA, Adole VA, Jagdale BS, Pawar TB, Desale BS, Shinde RS. Efficient synthesis, spectroscopic and quantum chemical study of 2,3-dihydrobenzofuran labelled two novel arylidene indanones: a comparative theoretical exploration. Mat. Sci. Res. India 2020;17:146–61.
[42] Pearson RG. Absolute electronegativity and hardness: applications to organic chemistry. J. Org. Chem. 1989;54:1423–30.
[43] Frisch MJ. Gaussian 03 Revision E.01. Wallingford CT: Gaussian Inc.; 2004.
[44] Jorgensen JH, Turnidge JD. Susceptibility test methods: dilution and disk diffusion methods. Manual of clinical microbiology 2015:1253–73.
[45] Johnson EM, Cavling-Arendrup M. Susceptibility test methods: yeasts and filamentous fungi. Manual of Clinical Microbiology 2015:2255–81.